Precise determination of the relative wave propagation parameters of similar events using a small-aperture seismic array

Javier Almendros, Enrique Carmona, and Jesús Ibáñez
Instituto Andaluz de Geofísica, Universidad de Granada, Granada, Spain

Received 5 December 2003; revised 24 August 2004; accepted 30 August 2004; published 25 November 2004.

[1] We propose a method to determine accurately the relative wave propagation parameters (apparent slowness and propagation azimuth) of a cluster of seismic events with similar waveforms recorded on a seismic array. This relative slowness estimate (RelSE) method is based on precise measurements of the delays among arrivals of different earthquakes to each of the array receivers. Delays are determined using interpolations of the cross-correlation functions of the earthquake waveforms. Accurate relative slowness vectors are estimated using a least squares fit of the observed delays to the delays corresponding to the arrivals of plane wave fronts. We tested the method using both synthetics and real data, in order to understand its resolution capabilities in presence of seismic noise and to assess the uncertainty regions associated with the slowness vector estimates. From these analyses, we establish a procedure to determine the 90% uncertainty regions associated with the estimates of relative slowness vectors. As an example of application of the RelSE method, we analyzed a multiplet composed of 16 similar earthquakes recorded during the 1999 seismic crisis at Deception Island volcano, Antarctica. Using a conventional slowness estimate method produces virtually the same result for every earthquake, because of the large uncertainties. Alternatively, using the RelSE method reduces the uncertainties of the estimates and allows to resolve the detailed distribution of (relative) apparent slowness vectors. Our results show that the slowness vectors are aligned within a narrow, north-south trending band, which represents a clue toward the features of the source region and/or source distribution. We repeated the procedure using different earthquakes as master events. The estimated distribution of slowness vectors is similar in every case, which demonstrates that our results are independent of the choice of reference event. *INDEX TERMS:* 7299 Seismology: General or miscellaneous; 7203 Seismology: Body wave propagation; 7215 Seismology: Earthquake parameters; 7230 Seismology: Seismicity and seismotectonics; 7280 Seismology: Volcano seismology (8419); *KEYWORDS:* seismic arrays, slowness vectors, multiplet analysis, Deception Island volcano

Citation: Almendros, J., E. Carmona, and J. Ibáñez (2004), Precise determination of the relative wave propagation parameters of similar events using a small-aperture seismic array, *J. Geophys. Res.*, *109*, B11308, doi:10.1029/2003JB002930.

1. Introduction

[2] Resemblance among seismic waveforms has been extensively exploited in several fields of seismology. There are essentially two situations in which similar seismograms are likely to be recorded. The first one requires two seismometers deployed at nearby locations; because of the close proximity of the receivers, we expect that any earthquake would yield a couple of highly correlated seismograms. The second one requires the use of a single seismometer and to wait till the Earth produces two quasi-identical earthquakes, something that, surprisingly enough, is not as rare as it sounds. Although these ideas may seem naive, they contain the seeds of two seismological techniques that have advanced very quickly during the past years: the use of seismic arrays and analyses of multiplets.

[3] Seismic arrays are dense, two-dimensional deployments of seismometers intended for recording and analyzing coherent wave fields. Array seismograms look similar because they are recorded at very close receivers. Differences among them consist mainly in phase delays produced by wave propagation. Thus seismic arrays are useful to determine the wave propagation parameters (apparent slowness and azimuth) of signals propagating across the array area. They are particularly appropriate for the analysis of complex wave fields [*Goldstein and Archuleta*, 1987; *Chouet*, 1996a; *Almendros et al.*, 2002a; *Chouet*, 2003]. Applications of seismic arrays for the analysis of wave fields recorded on volcanic areas have been especially numerous and fruitful. They have been used for example to investigate the composition of volcanic tremor [*Ferrazzini*

0148-0227/04/2003JB002930$09.00

et al., 1991; *Saccorotti et al.*, 2001b], to separate and analyze the different components contributing to the wave field [*Del Pezzo et al.*, 1997; *La Rocca et al.*, 2001; *Saccorotti et al.*, 2001b; *Almendros et al.*, 2001b], to separate source and path effects [*Chouet et al.*, 1997; *Saccorotti et al.*, 2001c], to track and locate seismo-volcanic sources [*Goldstein and Chouet*, 1994; *Neuberg et al.*, 1994; *Ibáñez et al.*, 2000; *La Rocca et al.*, 2000; *Almendros et al.*, 2001a], and to study the shallow structure under the array [*Goldstein and Chouet*, 1994; *De Luca et al.*, 1997; *Chouet et al.*, 1998; *Saccorotti et al.*, 2001c].

[4] While the waveform resemblance used by array techniques is circumstantial, and guaranteed only by design (i.e., the close proximity of the seismic receivers), resemblance in multiplet analysis is associated with the occurrence of earthquakes having intrinsically similar characteristics. These groups of similar earthquakes are a common event in all kinds of environments: tectonic, geothermal, volcanic, etc. The main advantage of the enhanced waveform similarity is that we are able to determine very accurately the time delay between the occurrence of two earthquakes. This precise relative timing of multiplet earthquakes can be used to estimate relative locations of clusters of seismic sources [*Got et al.*, 1994; *Phillips*, 2000; *Stich et al.*, 2001; *Saccorotti et al.*, 2002; *Brancato and Gresta*, 2003]. Other applications of precise relative timing include studies of the origin of the coda [*Antolik et al.*, 1996; *Aster et al.*, 1996; *Got and Coutant*, 1997], temporal variations of velocity in tectonic [*Poupinet et al.*, 1984; *Haase et al.*, 1995] or volcanic settings [*Ratdomopurbo and Poupinet*, 1995; *Poupinet et al.*, 1996], and the detailed properties of the inner structure of the Earth [*Song and Richards*, 1996; *Poupinet et al.*, 2000].

[5] In this article we propose a method that benefits from waveform resemblance in both of the senses described above. It is intended to determine very accurately the differences in apparent slowness and propagation azimuth of similar earthquakes, that is, if one of them propagates slightly faster than the others or toward a slightly different direction. The method is based on precise relative timing of earthquake waveforms recorded at the receivers of a seismic array. For a cluster of closely spaced, similar events we can produce precise relative slowness and azimuth estimates, although the average slowness and azimuth of the cluster remains less accurately resolved. The calculation scheme is the same as in relative location methods, only that seismic networks and relative hypocenter locations are substituted by seismic arrays and relative apparent slowness vectors, respectively.

2. Method

2.1. Slowness Estimate Methods

[6] Let us suppose a seismic array composed of N stations at positions $\vec{r}_i$, where $i = 1 \ldots N$. In the plane wave front approximation, the arrival times of a signal propagating across the array are given by

$$t_i^m = t_0^m + \vec{r}_i \cdot \vec{s}_m, \tag{1}$$

where t_0^m is the arrival time of the wave front m to the origin of coordinates, $\vec{r}_i$ is the position of station i, and $\vec{s}_m$ is the apparent slowness vector that characterizes the propagation of the wave fronts. The modulus, S, and direction clockwise from north, A, of the apparent slowness vector correspond to the inverse of the apparent velocity and propagation azimuth of the waves, respectively. The delays among arrivals of a signal characterized by a slowness vector $\vec{s}_m$ to different stations of the seismic array are given by

$$\Delta t_{ij}^m = \Delta \vec{r}_{ij} \cdot \vec{s}_m, \tag{2}$$

where $\Delta t_{ij}^m = t_j^m - t_i^m$ is the difference of arrival times of signal m to stations i and j and $\Delta \vec{r}_{ij} = \vec{r}_j - \vec{r}_i$ represents the relative position of stations i and j.

[7] The comparison of these delays – corresponding to a plane wave – with the delays obtained from the seismic data allows us to estimate the apparent slowness vectors of the recorded signals. This estimate can be done in several ways that lead to a variety of array methods in the time and frequency domains. Although based on very different assumptions and techniques, most methods amount to the calculation of a certain magnitude $F(\vec{s})$ that depends on the apparent slowness vector and quantifies the similarity between the actual wave delays and the plane wave delays given by equation (2). The distribution of F in the slowness vector space is used to estimate the slowness vectors of the recorded wave field, usually by finding the slowness vector $\vec{s}_{\max}$ that provides a maximum of the selected magnitude, $F(\vec{s}_{\max}) = \max\{F(\vec{s})\}$. The shape of the F function on the slowness vector domain is related to the way in which each method deals with noise and gives a measure of the uncertainty of the slowness vector estimate. A narrow peak centered at a particular slowness vector would represent a well-defined solution, while a broad peak means that F is relatively insensitive to changes in the apparent slowness vector, and thus large uncertainties are to be expected.

[8] Several array methods are available in the literature, characterized by different definitions of F. An intuitive example of a magnitude that is able to evaluate the similarity between the actual wave delays and the delays produced by the arrival of a plane wave front is the inverse of the residual of the least squares fit

$$F_{LS}(\vec{s}) = \left(\frac{2}{N(N-1)} \sum_{i=1}^{N-1} \sum_{j=i+1}^{N} \left(\Delta t_{ij}^{measured} - \Delta \vec{r}_{ij} \cdot \vec{s} \right)^2 \right)^{-1/2}. \tag{3}$$

More elaborate methods take advantage of the properties of different functions (both in time and frequency domains) to reduce the uncertainty of the slowness vector estimates and increase the resolution capabilities. For instance, the average cross-correlation (ACC) method [*Del Pezzo et al.*, 1997; *Almendros et al.*, 1999] assumes a function

$$F_{CC}(\vec{s}) = \frac{2}{N(N-1)} \sum_{i=1}^{N-1} \sum_{j=i+1}^{N} CC_{ij} \left(\frac{\Delta \vec{r}_{ij} \cdot \vec{s}}{\Delta T} \right), \tag{4}$$

where CC_{ij} is the normalized cross correlation of traces i and j and ΔT is the sampling interval. The quantity in parenthesis depends on the slowness vector and represents

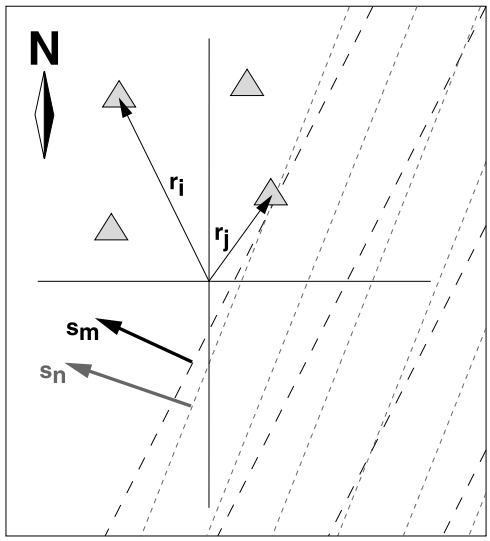

Figure 1. Sketch of the situation addressed by the RelSE method. Two wave fronts characterized by similar slowness vectors $\vec{s}_m$ and $\vec{s}_n$ incide upon a seismic array. The difference of slowness vectors $\vec{s}_n - \vec{s}_m$ can be estimated from the relative wave front delays at the array stations.

the number of samples that the traces are delayed before calculating CC_{ij}. Another example is the multiple signal classification (MUSIC) method [*Schmidt*, 1986; *Goldstein and Archuleta*, 1991]. This method is specifically designed to deal with noise and simultaneous arrivals of several wave fronts. The selected function is in this case

$$F_{MU}(\vec{s}) = \left(\sum_{k=Q+1}^{N} |\vec{a}(\vec{s}) \cdot \vec{v}_k|^2 \right)^{-1}, \qquad (5)$$

where $\vec{a}$ is defined by $a_j = \exp(i2\pi f \vec{r}_j \cdot \vec{s})$, $j = 1 \ldots N$; Q is the number of incoming signals; and $\vec{v}_k$, with $k = Q + 1 \ldots N$, represents a subset of $N - Q$ eigenvectors of the $N \times N$ covariance matrix of the array traces corresponding to small eigenvalues, that are used to define the noise subspace (see *Goldstein and Archuleta* [1991] for details).

[9] In general, high-resolution methods such as MUSIC provide narrower peaks of the $F(\vec{s})$ distributions and better accuracy of the slowness vector estimates. But, depending on the particular situation, different methods might be preferred. In any case, the choice of a method is not the only factor that controls the shape of $F(\vec{s})$. The spatial and temporal samplings of the wave field (array aperture and configuration, sampling interval), characteristics of the seismic signal (frequency content, amount of seismic noise), and presence of local heterogeneities beneath the array site (producing waveform distortions and station delays) impose severe constraints on our capability to obtain precise estimates of slowness vectors from array data. As an example, the typical size of the uncertainty region in the slowness vector domain for a signal with a frequency of a few Hz recorded with good signal-to-noise ratio on a dense seismic array with aperture of a few hundred meters deployed on a volcanic setting is ~0.2 s/km [*Chouet et al.*, 1997, 1998; *Almendros et al.*, 2000, 2001a; *Saccorotti et al.*, 2001a, 2001b].

2.2. RelSE: A Relative Slowness Estimate Method

[10] Uncertainties in the slowness vector estimates obtained with usual array methods are adequate for many applications. However, in the case of earthquake multiplets, we can improve drastically the accuracy of our estimates using a relative approach based on waveform similarity. In the following, we introduce the relative slowness estimate (RelSE) method, that constitutes an application of precise relative timing to data recorded on small-aperture seismic arrays. The key issue which constitutes the motivation for the method proposed is that waveform resemblance among multiplet earthquakes recorded at a single seismometer is generally better than waveform resemblance among seismograms of a single

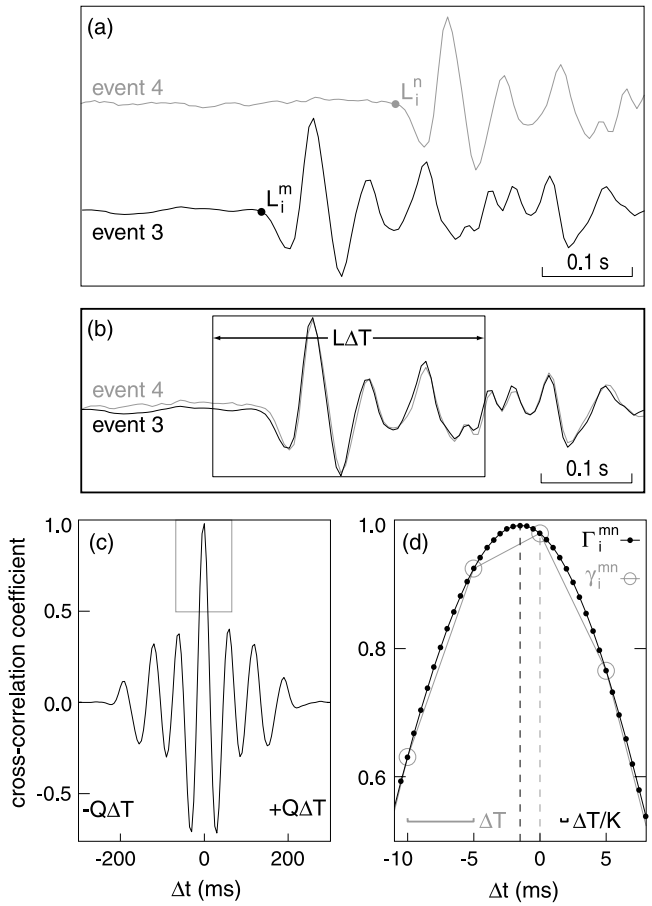

Figure 2. Example of the procedure to determine accurate delays using the interpolation of a CC function. (a) Seismograms of two earthquakes recorded at the same station. The samples labeled L_i^m and L_i^n identify a similar feature, in this case the P wave onset. (b) Seismograms aligned by removing the earthquake and propagation delays. The box represents the analysis window of duration $L\Delta T$. (c) CC function of the two traces, γ_i^{mn}, calculated for lag times between $-Q\Delta T$ and $Q\Delta T$, with $Q = 60$. (d) CC function γ_i^{mn} and its interpolated version Γ_i^{mn}, obtained using $K = 10$ (see text for explanations).

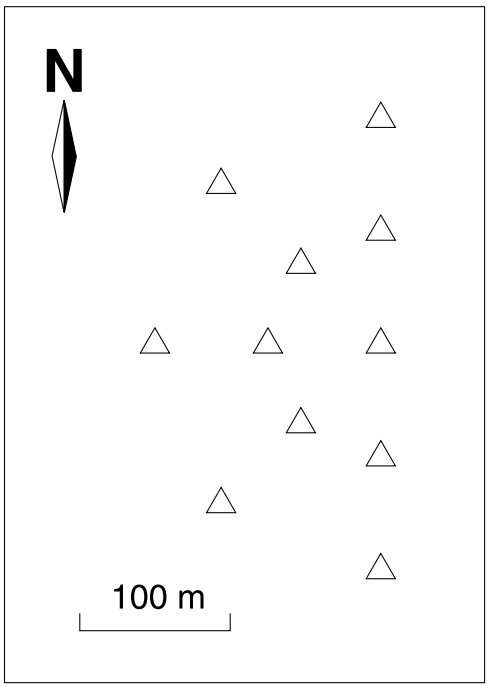

Figure 3. Configuration of the synthetic seismic array used for the tests of the RelSE method.

earthquake recorded at different array receivers, even for small-aperture arrays. Therefore we are able to measure the delay between arrivals of two similar events to the same station with higher accuracy than the delay between arrivals of a single earthquake to different seismic stations.

[11] Let us suppose two wave fronts propagating across a seismic array with slightly different apparent slowness vectors $\vec{s}_m$ and $\vec{s}_n$ (Figure 1). The RelSE method is designed to estimate with high accuracy the difference of slowness vectors $\vec{s}_n - \vec{s}_m$. If the wave fronts are produced by similar earthquakes belonging to a multiplet, we can determine very precisely the delays $\Delta t_i^{mn} = t_i^n - t_i^m$, that represent differences of the arrival times of two earthquakes m and n to the same station i. Estimates of delay times of events with similar waveforms can be achieved with accuracy beyond the sampling interval using two basic approaches. The first one is the cross-spectrum (CS) method, a frequency-domain method that calculates the slope of the phase of the cross spectrum [*Fremont and Malone*, 1987; *Ito*, 1990; *Got et al.*, 1994; *Ratdomopurbo and Poupinet*, 1995; *Poupinet et al.*, 1996; *Got and Coutant*, 1997; *Lees*, 1998]. The second is the cross-correlation (CC) method, that works in the time domain and uses an interpolation of the CC function to determine the delays among wave arrivals [*VanDecar and Crosson*, 1990; *Deichmann and Garcia-Fernandez*, 1992; *Mezcua and Rueda*, 1994; *Shearer*, 1997; *Saccorotti et al.*, 2002]. The choice of an approach depends on the degree of waveform similarity, frequency content of the signals, and signal-to-noise ratio (SNR). In general, since coherency depends critically on the presence of noise and decays faster for higher frequencies, the CS method yields best results for low-frequency signals with high SNR. On the contrary, the CC method is more stable and robust in those situations where signals have relatively low SNR [*Augliera et al.*, 1995; *Cattaneo et al.*, 1997].

[12] The delays Δt_i^{mn} are related to the station positions and apparent slowness vectors of the incident signals by

$$\Delta t_j^{mn} - \Delta t_i^{mn} = \Delta t_{ij}^n - \Delta t_{ij}^m = \Delta \vec{r}_{ij} \cdot \Delta \vec{s}_{mn} \tag{6}$$

where $\Delta \vec{s}_{mn} = \vec{s}_n - \vec{s}_m$ is the difference between the slowness vectors corresponding to the two signals. In order to estimate this difference of slowness vectors, we define for each pair of arriving wave fronts m and n a function similar to equation (3) that represents the inverse of the residual of the least squares fit of the measured $\Delta t_j^{mn} - \Delta t_i^{mn}$ to a plane wave front

$$F_{mn}(\vec{s}) = \left(\frac{2}{N(N-1)} \sum_{i=1}^{N-1} \sum_{j=i+1}^{N} \left(\Delta t_j^{mn} - \Delta t_i^{mn} - \Delta \vec{r}_{ij} \cdot \vec{s} \right)^2 \right)^{-1/2} \tag{7}$$

The best estimate of the difference of slowness vectors of the two signals corresponds to the value of $\vec{s}$ that yields the maximum of this F_{mn} function.

2.3. Implementation of the RelSE Method

[13] The application of the RelSE method to a multiplet of similar events consists of the following three steps.

2.3.1. Slowness Vector of the Master Event

[14] The first step is to calculate an independent estimate of the slowness vector of one of the multiplet members, $\vec{s}_m$,

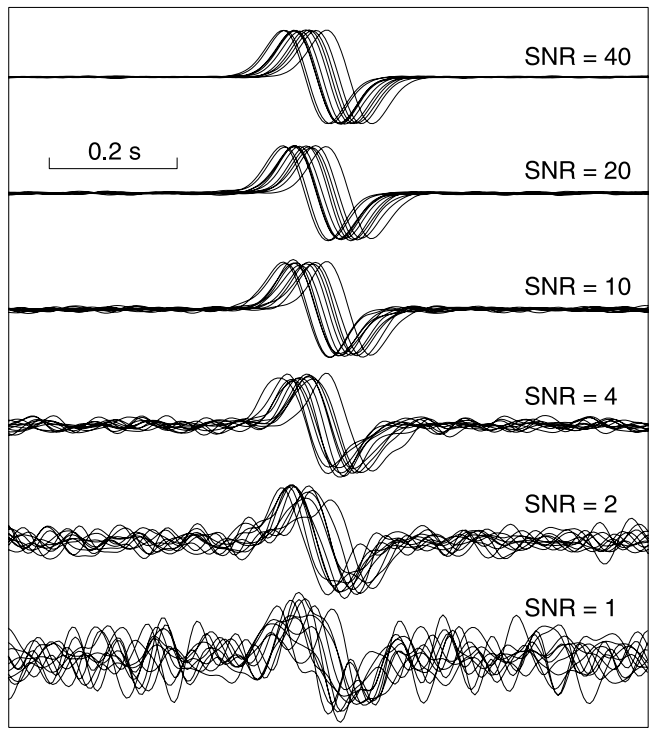

Figure 4. Examples of synthetic seismograms generated to simulate the arrival of a plane wave front characterized by an apparent slowness of 0.25 s/km and azimuth of 30° to the seismic array in Figure 3, for different levels of noise.

which will be used as a master event. For this task, we may use any conventional array technique.

2.3.2. Precise Measurements of Delay Times

[15] The second step is measuring the delay times Δt_i^{mn} between the master event and other multiplet members at every station of the array. Since we are interested just in the delays related to small differences of slowness vectors, we start by removing other effects. First of all, we determine the earthquake delay (ED), which is the time span between the occurrence of the two earthquakes. ED is measured at one of the traces for the master and secondary events by selecting samples L_i^m and L_i^n (Figure 2a) that identify a similar feature in both seismic events, for example the *P* wave onset. Correcting for ED (Figure 2b) means assuming that the earthquakes have occurred simultaneously.

[16] Additional delays for the remaining traces, due to wave propagation across the array, are given in the plane wave front approximation by equation (2). We refer to them as propagation delays (PD). PDs are calculated using the slowness vector of the master event, that for the moment constitutes our best estimate of the slowness vectors of the whole multiplet. Correcting for PD constitutes a procedure named "seismogram alignment" by *Goldstein and Archuleta* [1991]. It represents a translation of the origin in the slowness vector domain, which becomes situated just at the slowness vector of the master event. Therefore the calculated slowness vectors are relative to the master slowness vector.

[17] After correcting for ED and PD, any remaining delays constitute clues toward the relative apparent slowness vector. The precise determination of relative slowness vectors relies upon our ability to measure these residual delays as precisely as possible. In the RelSE method, accurate measurements of delay times are obtained from interpolations of the CC functions of the seismograms corresponding to the master and secondary events. We select an analysis window of length $L\Delta T$ containing the portion of the signal of interest (Figure 2b). CC functions between the master and secondary events at each station, γ_i^{mn}, are then calculated for time lags in a range of $\pm Q$ samples (Figure 2c). Rough estimates of the delays can be obtained from the position of the maxima of these functions, although more accurate values can be obtained by interpolation. Each sampling interval is divided in K intervals. CC values at the K-1 new sampling times are calculated using spline interpolation [*Press et al.*, 1992], keeping the values of the actual samples. This operation produces the interpolated CC functions Γ_i^{mn} (Figure 2d), and effectively means that the CC function, originally defined at $2Q + 1$ samples, is defined now at $2QK + 1$ samples. That is, we multiply by K the sampling frequency. The maxima of these Γ_i^{mn} provide accurate estimates of the delays between the master and secondary events at every station of the seismic array.

2.3.3. Determination of the Maximum of F_{mn}

[18] The third step in the application of the RelSE method consists in using equation (7) with the measured time delays. The differences of delays at two stations are given by

$$\Delta t_j^{mn} - \Delta t_i^{mn} = \left(\mu_j - \mu_i\right)\Delta T/K, \tag{8}$$

where μ_i represents the interpolated sample in which Γ_i^{mn} reaches its maximum. These values are introduced into equation (7) to obtain the distribution of $F_{mn}(\vec{s})$ in the slowness vector domain. The relative slowness vector corresponding to the maximum of F_{mn} is determined by grid search. This vector is our best estimate of the difference of slowness vectors $\Delta\vec{s}_{mn}$. Therefore the slowness vectors of secondary events can be calculated as

$$\vec{s}_n = \vec{s}_m + \Delta\vec{s}_{mn}. \tag{9}$$

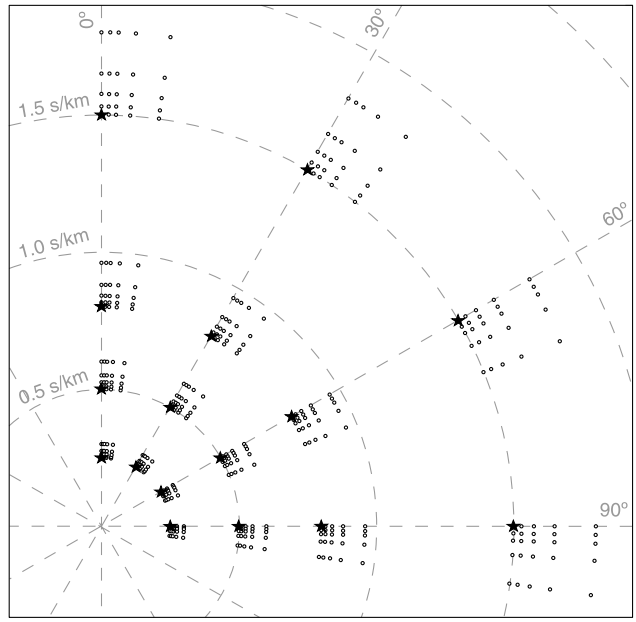

Figure 5. Sketch of the slowness vectors selected for the tests. For each of the 16 groups, the star represents the slowness vector of the master event, $\vec{s}_m$. Dots mark the slowness vectors $\vec{s}_n$ of the 25 events that we compare to the master event using the RelSE method.

3. Tests of the RelSE Method

[19] In order to test the capabilities of the RelSE method, we applied it both to synthetic and real data. In the first case, we generated two sets of similar seismograms W_i^m and W_i^n, $i = 1 \ldots N$, corresponding to the arrivals of signals characterized by apparent slowness vectors $\vec{s}_m$ and $\vec{s}_n$, respectively, to the stations of a seismic array. In the second case, real noise was added to a real earthquake recorded at a seismic array. We applied the RelSE procedure to these data and considered the results to understand the resolution performance and to assess the confidence regions associated with the solutions provided.

3.1. Synthetic Environment

[20] Synthetic seismograms were produced for a seismic array composed of 11 receivers distributed in a semicircular configuration with aperture of 300 m (Figure 3). We assumed a sampling interval of 5 ms. The signals are Ricker wavelets defined by

$$X(t, \tau_0) = A\left(\frac{t - \tau_0}{\tau}\right)\exp\left(-\left(\frac{t - \tau_0}{\tau}\right)^2\right) \tag{10}$$

where A is a constant, τ_0 is the delay of the signal from the origin time and τ is a measure of the pulse width. We

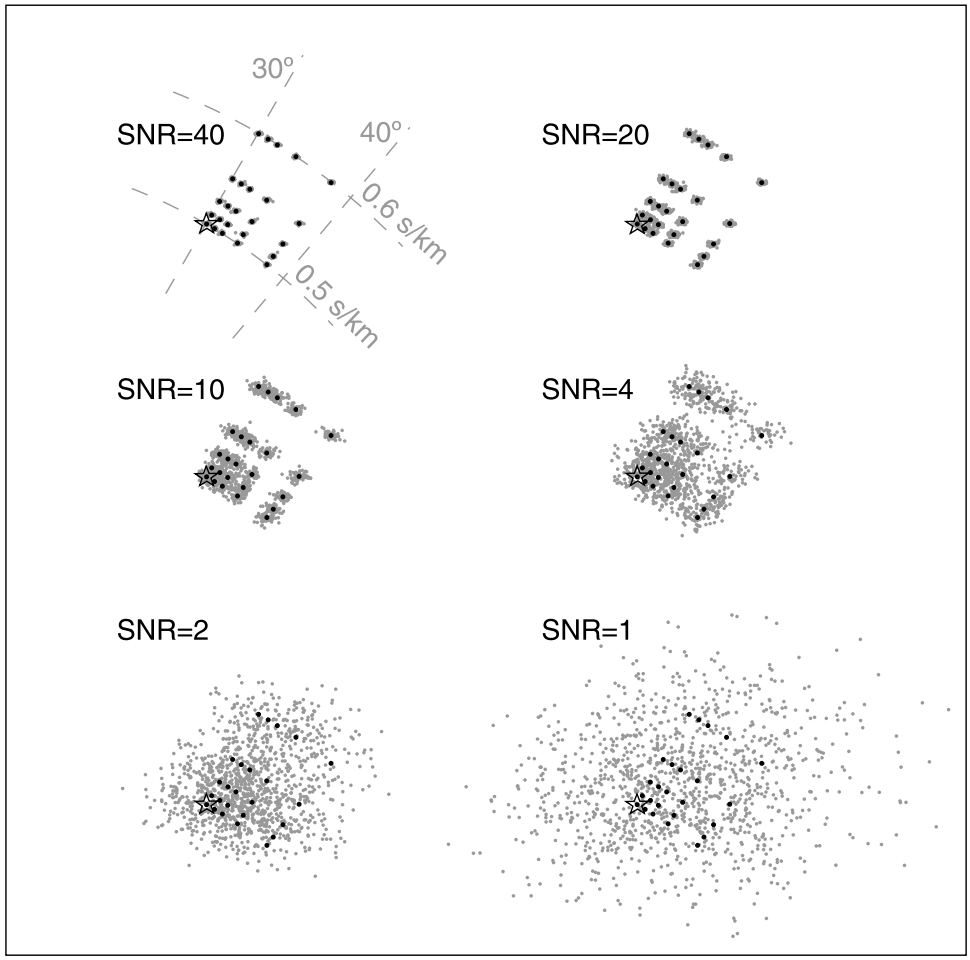

Figure 6. Examples of the results obtained from the relative slowness estimates of similar earthquakes using a master event with S_m = 0.5 s/km and A_m = 30°, for different levels of noise. Solid dots show the theoretical solutions, while grey dots mark estimates obtained by application of the RelSE method to different sets of noisy traces. The star shows the slowness vector of the master event.

selected $A = -\sqrt{2e}$ and τ = 0.05 s for a signal with positive first motion, maximum amplitude equal to unity and duration of about 0.2 s. To simulate a signal characterized by a slowness vector $\vec{s}$, seismograms were delayed by an amount defined by equation (1) for the particular set of propagation parameters assumed. Therefore the initial time τ_0 becomes a function of the apparent slowness vector $\vec{s}$ and the station position $\vec{r}_i$. We selected the central station of the array as the origin of coordinates and set the origin of time at 4 s before the arrival of the signal to the origin. Consequently, the arrival time to station i is given by

$$\tau_i(\vec{s}) \equiv \tau_0(\vec{s}, \vec{r}_i) = \vec{r}_i \cdot \vec{s} + 4 \text{ s}. \tag{11}$$

[21] We added incoherent noise to the traces. The noise samples were generated by filtering random time series of numbers between −1 and 1 in the 0.5–15 Hz band and renormalizing to maximum amplitude 1. Although simplistic, we think this model of seismic noise is appropriate for the present application. After all, we are comparing seismic waveforms recorded at the same station but at different times determined by the occurrence of the multiplet earthquakes. Repeating waveforms might happen in the noise wave field, for example associated with bursts of cultural noise. But there is no reason to think that these repeating waveforms will occur simultaneously with the earthquakes. Nevertheless, we also test the method using real noise and compare the results with those obtained using this simplistic noise model (see section 3.4).

[22] The final seismogram at station i is composed of signal and noise as follows

$$W_i(t, \vec{s}) = X(t, \tau_i(\vec{s})) + \frac{1}{\text{SNR}} \xi(t), \tag{12}$$

where $\xi(t)$ represents a pink noise time series and SNR is the signal-to-noise ratio. Figure 4 shows an example of the seismograms generated at the different stations of the synthetic array for different values of SNR.

3.2. Resolution and Effect of Noise

[23] We performed a series of tests of the RelSE method using two sets of seismograms generated for the synthetic array with different slowness vectors. We selected a grid of 16 slowness vectors $\vec{s}_m$ for the master event, defined by apparent slownesses of S_m = 0.25, 0.5, 0.8, and 1.5 s/km and propagation azimuths of A_m = 0, 30, 60, and 90° (stars in Figure 5). For each slowness vector $\vec{s}_m$ = (S_m, A_m), we

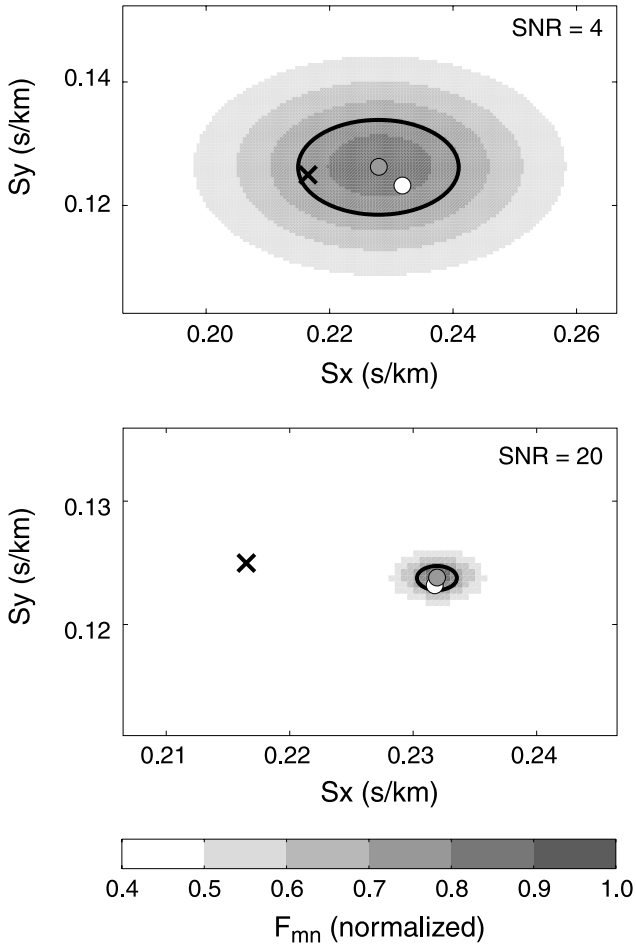

Figure 7. Distribution of F_{mn} in the slowness vector domain for SNRs of (top) 4 and (bottom) 20, showing the maximum used to define the relative slowness vector estimate. In both cases a cross marks the position of the master event slowness vector; an open dot represents the slowness vector of the secondary event; and a shaded dot indicates the position of the maximum of F_{mn} and therefore our best estimate of the slowness vector corresponding to the secondary event.

defined the slowness vectors of the secondary events, $\vec{s}_n = (S_n, A_n)$, using a second grid of 25 slowness vectors. They represent propagation parameters similar to $\vec{s}_m$ and are given by

$$S_n = S_m(1 + dS) \quad , \quad A_n = A_m + dA \tag{13}$$

where dS = 0, 0.02, 0.05, 0.1, and 0.2 and dA = 0, 1, 2, 4, and 8° (dots in Figure 5). We generated seismograms corresponding to the master and secondary events with six different SNRs of 40, 20, 10, 4, 2, and 1. In order to properly represent the random nature of noise, and have a statistically meaningful ensemble, we generated in every case 50 different sets of traces corresponding to the slowness vector $\vec{s}_n$, in which the signal X is exactly the same but with different realizations of ξ (see equation (12)). We applied the RelSE method to a window of 0.3 s centered at the wave arrival at 4 s from the first sample, with the parameters Q = 30 and K = 20 (see section 2.2). The traces were filtered using a weak zero-phase filter in the range 1–25 Hz. In order to optimize the grid search of the maximum of F_{mn}, we defined four slowness domain sizes and grid spacings that were applied successively. Each domain was centered at the provisional maximum obtained with the previous domain, starting at (0, 0) that represents the slowness vector of the master event. In this way, we reduce the computation times and speed up the process. We selected sizes of 4, 1, 0.2, and 0.03 s/km and grid spacings of 0.2, 0.04, 0.008, and 0.0001 s/km, respectively.

[24] This procedure resulted in 6 × 16 × 25 × 50 = 120000 applications of the RelSE method. Figure 6 summarizes part of the results, corresponding to the estimates of the slowness vectors of the secondary events with respect to a master event characterized by slowness of S_m = 0.5 s/km and azimuth of A_m = 30°, for the different SNRs considered. For high SNR, when the waveforms are not significantly altered by the presence of noise, the resolution capabilities of the method are excellent. On the contrary, for signals with low SNR, the waveform similarity is so small (see Figure 4) that the method is not able to provide accurate solutions. In any case, we confirm that our relative approach improves greatly the resolution performance of absolute array methods. For example, for a SNR of 10 we are able to resolve clearly solutions separated just 0.03 s/km in apparent slowness or 2° in azimuth.

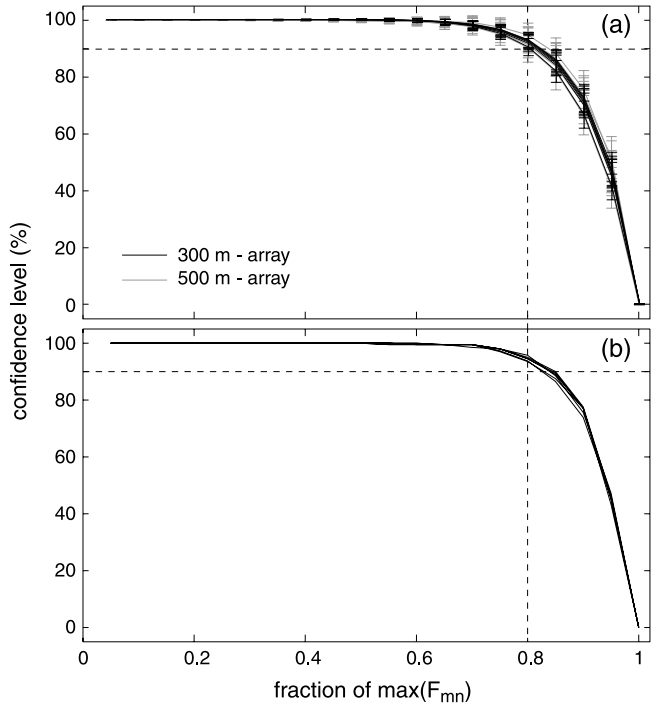

Figure 8. Percentage of slowness vector solutions contained within the isocontours corresponding to different levels of F_{mn} versus the levels that define the isocontours. (a) Results from synthetic tests using arrays with apertures of 300 (black) and 500 m (gray). There is one line for each SNR. The plots are averages of the results for all the slownesses and azimuths considered in the tests. Error bars indicate the standard deviations. (b) Results from the tests performed using real data. There is one line for each SNR.

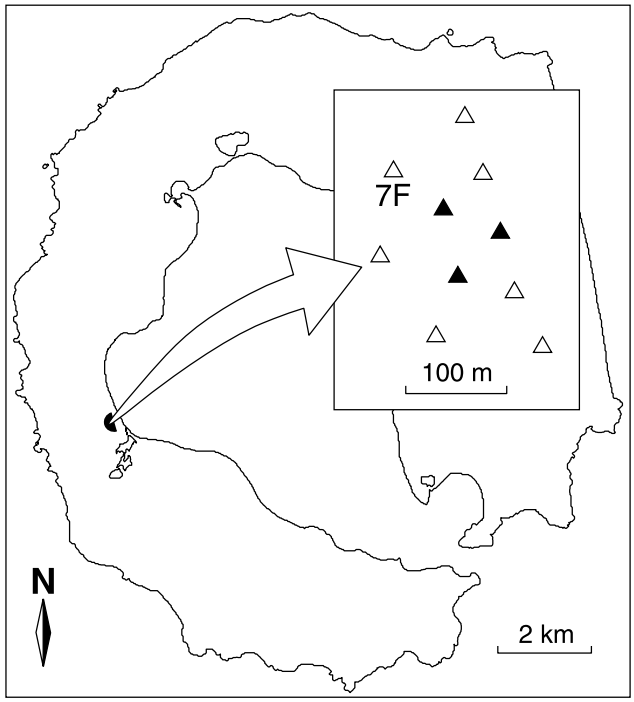

Figure 9. Map of Deception Island volcano, Antarctica, showing the location and configuration of the seismic array operating at Fumarole Bay during the 1999 seismic crisis. Solid triangles represent three-component seismometers, and open triangles are vertical sensors. The label 7F marks the station where the seismograms shown in Figure 10 have been recorded.

[25] The effect of noise and its influence on the resolution capabilities of the RelSE method can be better understood by looking at the shape of $F_{mn}(\vec{s})$. As an example, Figure 7 shows distributions of F_{mn} for events characterized by identical $\vec{s}_m$ and $\vec{s}_n$ but different SNRs. High SNR values yield narrow peaks that provide high slowness resolution, while low SNRs always yield low, broad peaks that are relatively insensitive to changes in slowness.

3.3. Definition of Confidence Limits

[26] The distributions of $F_{mn}(\vec{s})$ produced by the RelSE method not only reveal the best estimates of relative slowness vectors, but also point out the uncertainties of these estimates. The former information is obtained from the position of the maxima in the slowness domain, while the latter can be determined from their shape.

[27] Our tests suggest a direct relationship between the shape of F_{mn} and the magnitude of the estimated errors (i.e., the difference between the real and calculated slowness vectors). Large errors are always related to estimates whose F_{mn} functions display low, broad peaks, while small errors are linked to high, narrow F_{mn} peaks (Figure 7). In order to quantify this idea and assess the confidence limits associated with the relative slowness vector estimates, we investigated the percentage of test solutions for which the true slowness vector was contained within a given isocontour of the corresponding $F_{mn}(\vec{s})$ surface (Figure 8a). If we wish to ensure a reasonable confidence of 90%, we should select a value of 0.80 times the maximum of F_{mn}. Therefore 80% of the maximum F_{mn} constitutes an adequate choice for the assessment of confidence limits in the RelSE method.

[28] To check that this result is not affected by other factors such as the array aperture, we repeated the whole procedure described above for a seismic array with the same configuration as before (Figure 3) but with an aperture of 500 m. The

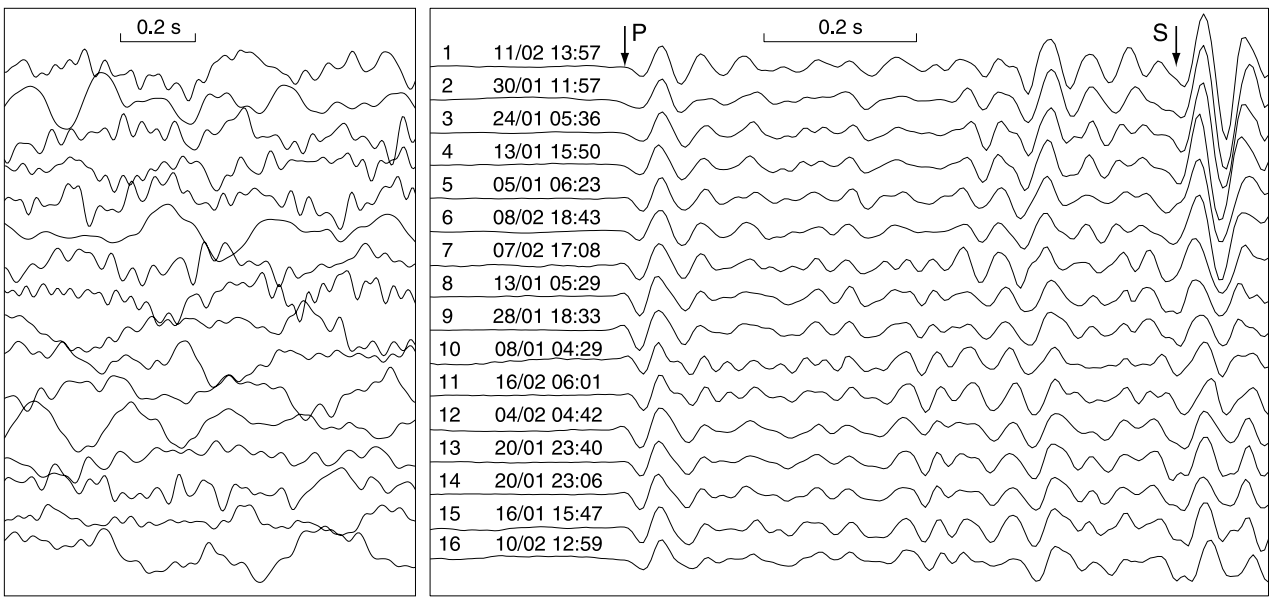

Figure 10. Seismograms of sixteen earthquakes recorded at station 7F of the Fumarole Bay array (see Figure 9) during the 1999 seismic swarm. The left panel shows normalized samples of pre-event noise recorded 2 s before the *P* wave arrival. The right panel shows the earthquake waveforms for 1 s after the *P* wave arrival. The *P* and *S* phases are labeled with arrows. Earthquake numbers refer to Table 1.

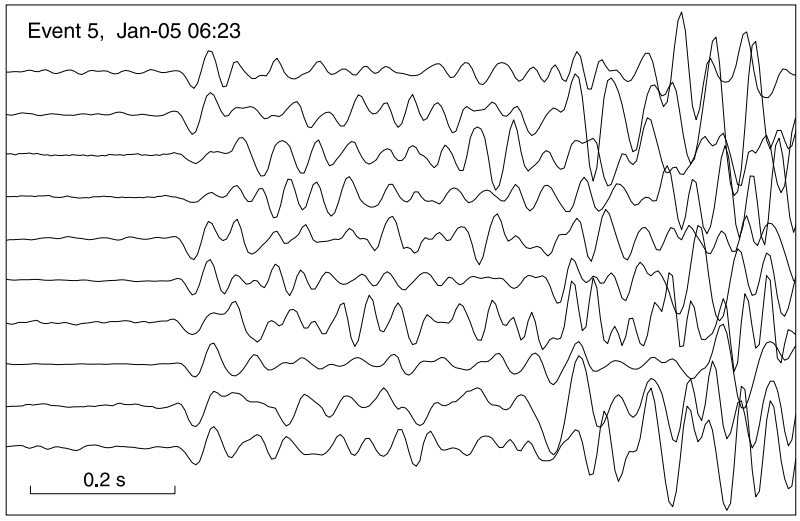

Figure 11. Seismograms corresponding to the earthquake marked as number 5 in Figure 10, recorded at all the sensors of the Fumarole Bay array.

results do not change significantly (Figure 8a), although for small slowness values we found a slight improvement due to the larger times needed to travel across the array.

3.4. Tests With Real Noise

[29] The synthetic signals generated to test the capabilities of the RelSE method may not be a perfect representation of the real wave fields. With this in mind, we proceeded to test the potential of the method with real data. The problem in this case is that there is no way to know what the real slowness vector is, and therefore we are not able to determine the errors. We solved this issue by calculating the slowness vector of an event relative to itself, which should obviously be zero. Any deviation would be an artifact due to the noise content.

[30] We selected the *P* wave arrival of an earthquake recorded at a seismic array (event 3; see section 4 below for details) and added different amounts of real noise recorded at the same array:

$$S' = S + \alpha \cdot N, \tag{14}$$

where S represents the original signal, N a noise sample, α the amount of extra noise, and S' the modified signal. Since S contains some noise already, the final SNR should be calculated as

$$\mathrm{SNR}' = \frac{S}{N + \alpha N} = \frac{\mathrm{SNR}}{1 + \alpha}. \tag{15}$$

We used α = 0.1, 0.2, 0.4, 1, 2, and 4, which correspond to modified SNRs between 6 and 22, approximately. For each α we repeated the calculations 200 times, using different samples of noise taken from several array records. As before, we investigated the percentage of test solutions for which the area defined by a given $F_{mn}(\vec{s})$ isocontour included the real solution – in this case, the origin of the relative slowness vector domain. We found that this percentage is equivalent to the case of purely synthetic events (Figure 8).

[31] Using these results, we define the error limits in the RelSE method as the region where F_{mn} takes values

Table 1. Estimates of Slowness Vectors for the 16 Events Analyzed Using the Conventional Average Cross-Correlation Approach

Event	Date	*P* Time	SNR	S_x, s/km	S_y, s/km	*S*, s/km	*A*, deg	CC_{max}
1	11 Feb.	1357:58.025	9	−0.20	−0.08	0.215	248	0.72
2	30 Jan.	1157:41.810	10	−0.22	−0.07	0.231	252	0.74
3	24 Jan.	0536:38.170	25	−0.24	−0.12	0.268	243	0.85
4	13 Jan.	1550:33.050	15	−0.26	−0.11	0.282	247	0.82
5	5 Jan.	0623:28.695	20	−0.24	−0.12	0.268	243	0.79
6	8 Feb.	1843:48.165	12	−0.30	−0.12	0.323	248	0.78
7	7 Feb.	1708:19.045	8	−0.30	−0.12	0.323	248	0.76
8	13 Jan.	0529:38.340	7	−0.24	−0.12	0.268	243	0.72
9	28 Jan.	1833:19.215	14	−0.24	−0.12	0.268	243	0.80
10	8 Jan.	0429:39.715	6	−0.27	−0.17	0.319	238	0.63
11	16 Feb.	0602:04.225	12	−0.27	−0.17	0.319	238	0.83
12	4 Feb.	0442:50.750	10	−0.27	−0.17	0.319	238	0.77
13	20 Jan.	2340:49.000	15	−0.24	−0.12	0.268	243	0.86
14	20 Jan.	2306:57.380	16	−0.24	−0.12	0.268	243	0.84
15	16 Jan.	1547:67.265	8	−0.25	−0.12	0.277	244	0.75
16	10 Feb.	1259:17.015	9	−0.24	−0.12	0.268	243	0.79

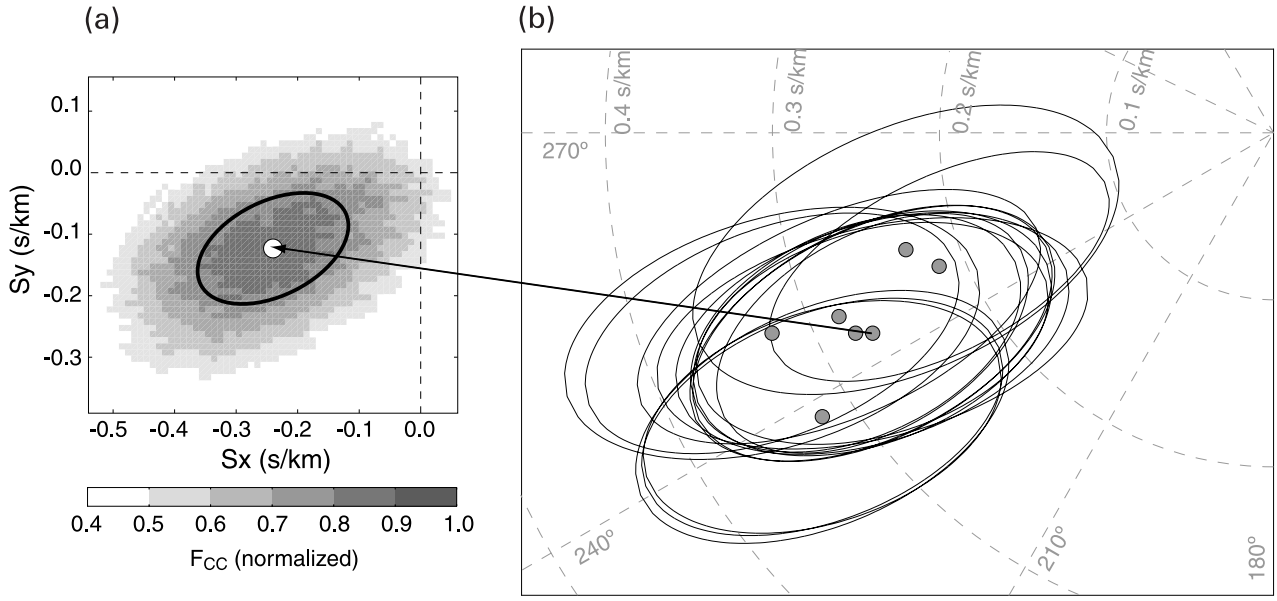

Figure 12. (a) Distribution of the array-average cross correlation in the slowness vector domain, F_{CC}, for event 13. The white dot marks the slowness vector corresponding to the maximum of F_{CC}. The thick line represents the 90% confidence region. (b) Results of the application of the conventional average cross-correlation method for the estimation of the slowness vectors corresponding to the *P* wave of the earthquakes shown in Figure 10. Ellipses indicate the 90% confidence regions. The arrow marks the solution for event 13 shown in Figure 12a.

larger than 80% of its maximum value. This can be expressed as

$$ERR(\vec{s}) = \{\vec{s} \mid F_{mn}(\vec{s}) \geq 0.80 \max(F_{mn})\}. \quad (16)$$

4. Application to Real Data

[32] As an example of the results that the proposed procedure is able to provide, we apply the RelSE method to a selection of data recorded at Deception Island volcano, Antarctica, during the 1999 seismic crisis [*Ibáñez et al.*, 2003a, 2003b]. At that time, a short-period, small-aperture seismic array was operating in Fumarole Bay (Figure 9). The array was composed of 10 seismometers distributed in a semicircular configuration with aperture of ~300 m. The sampling rate was 5 ms. More than 2000 local earthquakes were recorded during a period of two months (January–February). Preliminary locations of 863 earthquakes have been obtained using conventional ACC estimates of the apparent slowness vectors combined with ray-tracing through the velocity model. The distances along the ray paths were determined by the S-P delays [*Ibáñez et al.*, 2003b].

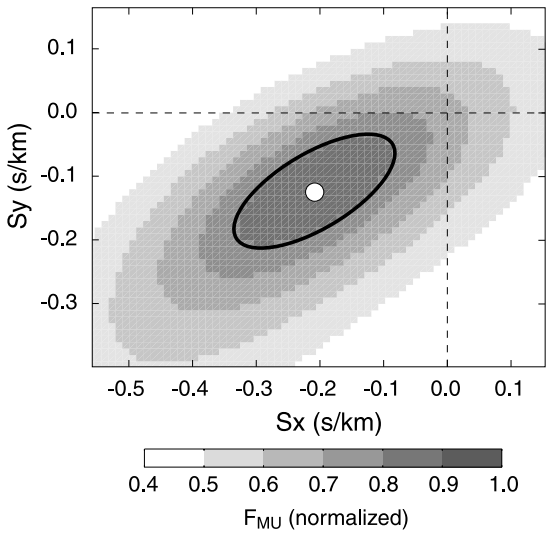

Figure 13. Distribution of the MUSIC power in the slowness vector domain, F_{MU}, for event 13. The open dot marks the slowness vector corresponding to the maximum of F_{MU}. The thick line represents the 90% confidence region.

Table 2. Estimates of Slowness Vectors for the 16 Events Analyzed Using the RelSE Method, Relative to Event 5

Event	S_x, s/km	S_y, s/km	S, s/km	A, deg	F_{max}, ms^{-1}
1	−0.2413	−0.0855	0.25595	250.45	0.40
2	−0.2547	−0.0910	0.27042	250.31	0.78
3	−0.2402	−0.0965	0.25882	248.08	0.75
4	−0.2368	−0.0950	0.25510	248.10	0.75
5	−0.2400	−0.1200	0.26833	243.43	...
6	−0.2538	−0.1017	0.27338	248.13	1.04
7	−0.2736	−0.1321	0.30379	244.20	0.40
8	−0.2412	−0.1406	0.27917	239.73	0.57
9	−0.2510	−0.1425	0.28861	240.38	0.54
10	−0.2507	−0.1583	0.29648	237.70	0.40
11	−0.2554	−0.1717	0.30774	236.06	0.43
12	−0.2543	−0.1508	0.29563	239.30	0.56
13	−0.2324	−0.1426	0.27265	238.43	0.51
14	−0.2446	−0.1453	0.28449	239.26	0.64
15	−0.2344	−0.1428	0.27446	238.62	0.41
16	−0.2487	−0.1582	0.29474	237.51	0.44

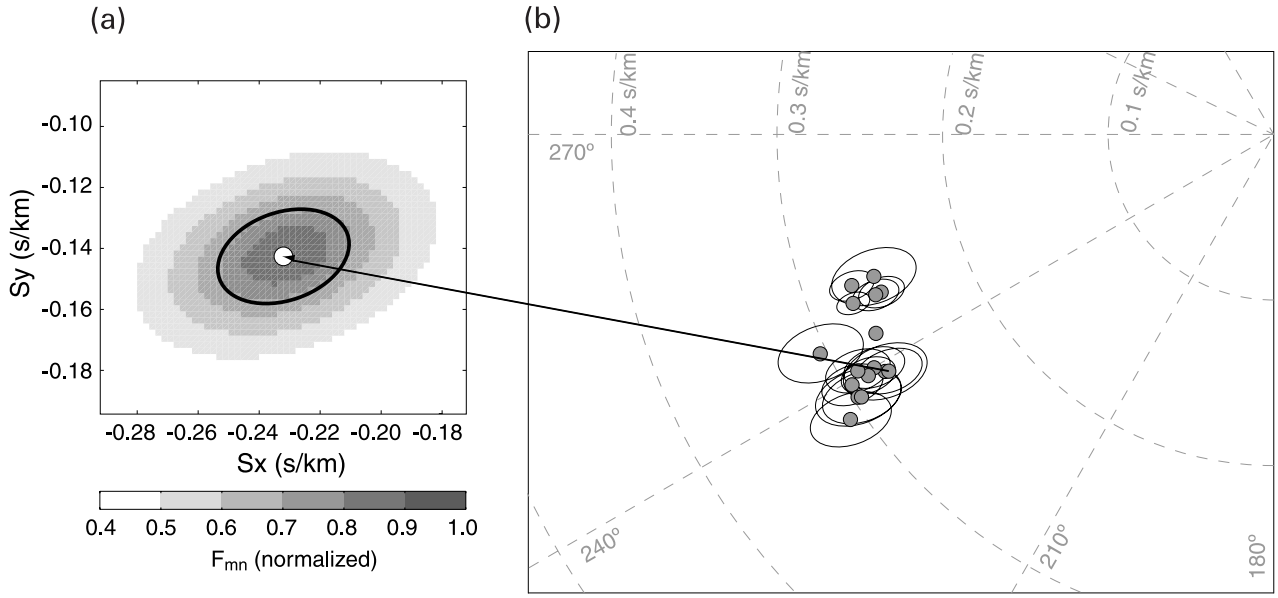

Figure 14. (a) Distribution of F_{mn} in the slowness vector domain for event 13. The open dot marks the slowness vector corresponding to the maximum of F_{mn}. The thick line represents the 90% confidence region. (b) Results of the application of the RelSE method for the estimation of the slowness vectors corresponding to the *P* wave of the earthquakes shown in Figure 10. Ellipses indicate the 90% confidence regions. The master event selected is event number 5 in Figure 10. The arrow marks the solution for event 13 shown in Figure 14a.

[33] For this work, we take advantage of the fact that some of the Deception Island earthquakes display very similar waveforms. Although site effects at a seismic station may induce resembling waveforms for virtually any earthquake, the occurrence of earthquakes with very different waveforms as well [*Ibáñez et al.*, 2003b] ensures that waveform similarity is intrinsically associated with the earthquake source. E. Carmona et al. (Characterization of fracture systems using precise array locations of earthquake multiplets recorded at Deception Island volcano, Antarctica, manuscript in preparation, 2004) grouped the earthquake data set in multiplets using the equivalence-class approach [*Aster and Scott*, 1993; *Maurer and Deichmann*, 1995] and a cross-correlation technique [*Saccorotti et al.*, 2002] that compares both the *P* and *S* waveforms recorded at the central station of the array. We selected one of these groups for the present analysis. The multiplet comprises sixteen members that occur along a time interval of more than a month. Figure 10 shows the corresponding seismograms recorded at one of the array stations. While pre-event noise displays very different waveforms, the similarity among the earthquakes is significant and lasts for several seconds. Conversely, Figure 11 shows the seismograms recorded at every array station for one of the events. Although there is some coherency among the traces, the waveforms are not alike, probably due to distortions produced in local heterogeneities under the array site. These plots illustrate the reason why a relative slowness estimate technique can provide more accurate results than its absolute counterpart, as discussed in section 2.2.

[34] Table 1 and Figure 12 show the results of the conventional ACC method applied to the estimate of the *P* wave slowness and azimuth. We used a slowness grid spacing of 0.01 s/km. Given the dimensions of the seismic

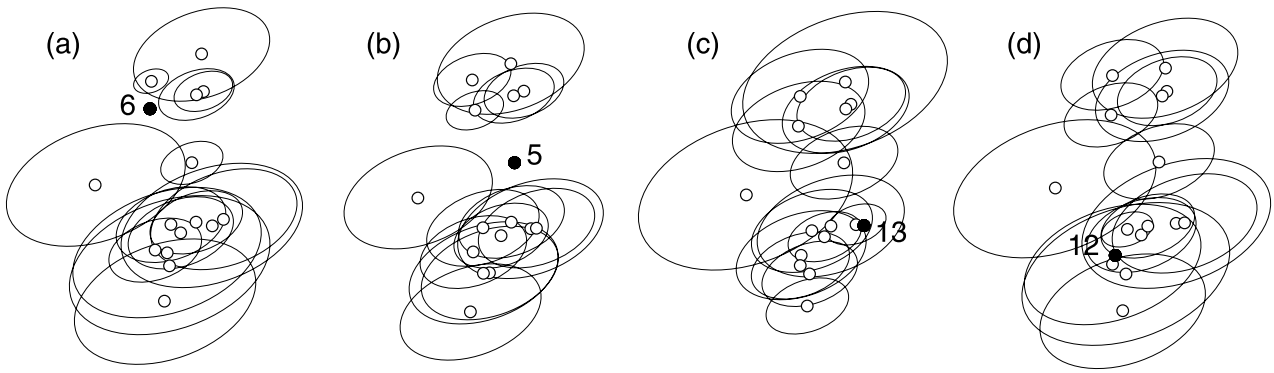

Figure 15. Comparison of the results obtained considering different earthquakes as master event (see Table 1): (a) event 6; (b) event 5; (c) event 13; (d) event 12.

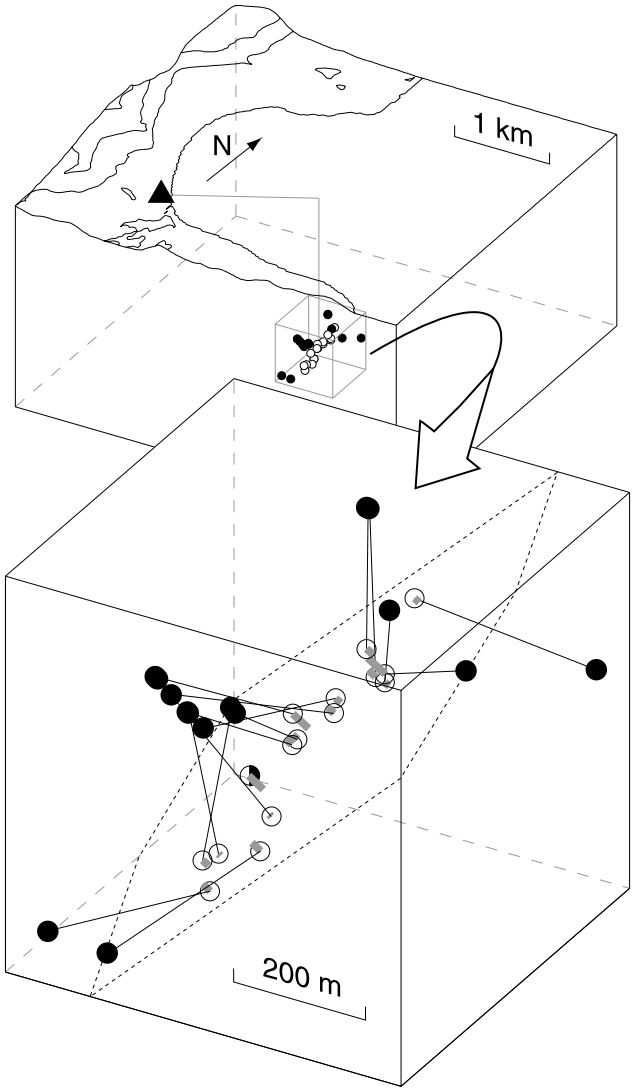

Figure 16. Comparison of ray tracing results using standard ACC (solid dots) and RelSE slowness vector estimates (open circles) for the selected earthquake multiplet. (top) General view of the Fumarole Bay region, showing the position of the seismic array (solid triangle) and the epicentral distance and depth of the source region (gray line). (bottom) Detailed view of the source region. For each earthquake, a black line joins the source locations obtained using the ACC and RelSE methods. For RelSE solutions, thick gray lines show the distance to the best fit plane indicated by the dotted line.

array and the sampling rate involved, a smaller variation in the slowness vector does not produce any change in the CCs and is not perceived by the array. Actually, the optimum grid spacing should be larger, because we have to consider also other effects such as the station density and presence of seismic noise (see, e.g., equation (12) from *Goldstein and Archuleta* [1991]). The absolute slowness vector estimates for the *P* waves of the multiplet events reveal that they propagate with slownesses of 0.22–0.32 s/km and azimuths of 243–252° from north. However, since the error regions are ellipses with approximate dimensions of 0.12 × 0.24 s/km, much larger than the range of variation of the solutions, we should not interpret the estimates in detail, but consider that we obtain basically the same solution for all sixteen events of the multiplet.

[35] For this particular earthquake multiplet, the application of a high-resolution frequency-slowness method such as MUSIC [*Schmidt*, 1986] does not improve significantly the results. The slowness vectors calculated with MUSIC are similar to the slowness vectors obtained with the ACC method and displayed in Figure 12. The exact values are not the same, but the approximate positions of the estimates and sizes of the error regions are alike. As an example, Figure 13 shows a slowness vector estimate performed using the MUSIC algorithm for event 13. Compare this plot with the left panel of Figure 12. In general, for seismograms that display a low level of noise, the results of the MUSIC and ACC methods are usually comparable. Nevertheless, the enhanced resolution capabilities of the MUSIC method are plainly evident when the data exhibit a low signal-to-noise ratio.

[36] We applied the RelSE method to the *P* wave onset of the multiplet earthquakes, using the same parameters as in the synthetic tests. We selected event 5 as master event, and obtained the results displayed in Table 2 and Figure 14. The solutions show apparent slownesses of 0.25–0.31 s/km and azimuths of 236–250°. The sizes of the error ellipses are greatly reduced to an average of about 0.03 × 0.05 s/km, which means that the confidence regions in the relative estimates have areas more than 20 times smaller than the confidence regions in the absolute estimates. We highlight that, although the relative slowness vectors have been accurately determined, the absolute estimates are not precisely known. The relative estimates should be considered as "floating" on the apparent slowness plane, since we still have to consider the uncertainty associated with the absolute estimate of the slowness vector of the master event.

[37] Figure 15 shows the relative slowness vectors obtained using different members of the multiplet as master events. Although there are small differences in the details, the relative positions of the estimated vectors remain the same. The method is robust enough so that the choice of reference event does not affect significantly the results.

5. Discussion

[38] The small sizes of the confidence regions shown in Figure 14 allow us to visualize a structure in the relative slowness vectors of the analyzed multiplet. They are distributed along a north-south trending band in the slowness vector domain, with varying density of solutions. This constitutes a hint toward the spatial distribution of earthquake sources, although the interpretation of detailed slowness vector data in terms of source locations is not trivial. However, if we assume simplifying hypotheses about the medium, such as lateral homogeneity and depth-increasing velocity, we could establish a link between the relative slowness vectors and relative source locations. Taking into account that the delays between the *S* and *P* wave arrivals are similar for all the earthquakes (about 0.7 s), a smaller apparent slowness of the *P* wave implies that the corresponding source location is deeper. Consequently, the features of the slowness vector distribution shown in Figure 14 might be explained if the

earthquakes originate at a fracture system located toward an azimuth of about 60° from the array site and show a southward increase of source depth. Because of the waveform similarity of the multiplet members, this system may indeed be regarded as a single crack dipping approximately to the south, although a more detailed analysis of the *S-P* times and a better knowledge of medium are needed to suggest further conclusions.

[39] Another observation supporting the accuracy of our estimates is that events with nearby slowness vectors show enhanced waveform similarity. For example, events 1–6, characterized by a larger relative amplitude of the *S* wave (Figure 10), are grouped together at the north end of the slowness vector band. The *S* wave amplitude seems to be more sensitive to small differences in source location among the multiplet members.

[40] This simple exercise illustrates that the accurate determination of relative slowness vectors opens up the possibility of performing relative source locations using multiplet data recorded on seismic arrays. Although in this case our reasoning was mostly based on qualitative arguments, quantitative analyses are also feasible. The combination of the RelSE method with an array location technique for a cluster of similar earthquakes would improve the results in two senses. First, the enhanced slowness resolution capabilities of the RelSE method would yield precise estimates of the relative slowness vectors. Therefore the location methods would provide more accurate relative source locations. Second, these array location methods depend on the assumed velocity structure of the medium. The waveform similarity of multiplet earthquakes ensures that most part of the path and site effects will be common. Therefore the uncertainties introduced in the relative locations by our imperfect knowledge of the medium could be reduced, although they remain in the absolute location of the master event.

[41] As an example, we use ray tracing to determine the relative source locations of the earthquake multiplet displayed in Figure 10. The data we need to know are: the apparent slowness vectors of the *P* wave arrivals; measurements of the S-P delay times; and a velocity model for the medium. In order to emphasize the performance of the RelSE method, we use both ACC and RelSE slowness vector estimates (Tables 1 and 2, respectively). The *S-P* times and velocity model are the same used by *Ibáñez et al.* [2003b]. Figure 16 shows the calculated source locations. ACC solutions (solid dots) were already obtained by *Ibáñez et al.* [2003b] in their analyses of the 1999 Deception Island earthquakes. They are contained within a small region northeast of the array site. No clear features are noticeable in this source distribution, most likely due to the large uncertainties associated with the ACC method. In fact, *Ibáñez et al.* [2003b] estimated the uncertainty of their locations in 500 m, larger than the average distance among the solutions given in Figure 16. Therefore the calculated ACC source locations should be basically regarded as coincident in a single position. On the contrary, RelSE solutions (open circles) are characterized by uncertainties of a few tens of meters. They appear in a thin, elongated cluster, defining approximately a plane dipping ~45° toward the southwest. The average distance from the source locations to the best fit plane is lower than 20 m. Although this plot constitutes a preliminary result, it suggests the possibility of using array data to determine precise relative source locations. Moreover, the RelSE method may add a new perspective to the problems for which the standard relative location techniques are useful, for example the determination of fracture geometries from microearthquake data, imaging of brittle regions in volcanoes, etc.

[42] Another potential application of the RelSE method is the analysis of long-period (LP) volcano seismicity. This type of seismicity is characterized by persistency of spectral features and occurrence of seismic events with similar waveforms. These facts have been related to nondestructive sources such as the resonance of cracks and conduits [e.g., *Chouet*, 1996b]. Seismic swarms of LP events with similar waveforms have been recorded at several volcanoes around the world [*Ibáñez et al.*, 2000; *Falsaperla et al.*, 2002]. In many cases, source locations can not be precisely estimated due to emergent onsets and/or unfavorable station distributions. Using seismic arrays allows for the estimates of approximate source locations of the LP seismicity [*Neuberg et al.*, 1994; *Almendros et al.*, 1999; *La Rocca et al.*, 2000; *Chouet*, 2003]. In particular, the source location technique developed by [*Almendros et al.*, 2001b] yields a 3D image of the sources of the seismo-volcanic activity [*Almendros et al.*, 2001a]. The image resolution of the source regions could be greatly improved with the use of the RelSE method.

[43] Although in section 4 we have applied the RelSE method just to the *P* wave onset of the earthquakes, it can be applied to other phases as well. The knowledge of the relative slowness vectors of seismic phases would add geometrical information – about azimuth and incident angles – to the temporal information – about time delays – considered so far in analyses of earthquake multiplets. This extra information could be very useful for a better understanding of the fine details of the Earth structure. Moreover, this method would not necessarily be restricted to conventional phases. Taking advantage of the ability of seismic arrays to detect and characterize any coherent wave front propagating across the array area [e.g., *Almendros et al.*, 2002b], RelSE analyses could comprise virtually the entire seismogram including the coda. Bearing this in mind, we anticipate very interesting applications of the RelSE method to the deterministic study of seismic scattering and coda generation.

[44] **Acknowledgments.** We thank F. Albarede, L. Steck, an anonymous editor, and two anonymous reviewers for their useful comments and suggestions. The data we have used were obtained during a seismic survey under project ANT-1111 of the Spanish Ministry of Science and Technology. We thank all participants in that survey for their help, and the Spanish Navy and Army for providing logistic aid. Partial support for the research was also provided by projects REN2001-3833/ANT and REN2001-2814-C04-04/RIES of the Spanish Ministry of Science and Technology, and by the European Union project EVR1-CT-2001-40021.

References

Almendros, J., J. M. Ibáñez, G. Alguacil, and E. Del Pezzo (1999), Array analysis using circular-wave-front geometry: An application to locate the nearby seismo-volcanic source, *Geophys. J. Int.*, *136*, 159–170.

Almendros, J., J. M. Ibáñez, G. Alguacil, J. Morales, E. Del Pezzo, M. La Rocca, R. Ortiz, V. Araña, and M. J. Blanco (2000), A double seismic

antenna experiment at Teide Volcano: Existence of local seismicity and lack of evidences of volcanic tremor, *J. Volcanol. Geotherm. Res.*, *103*, 439–462.

Almendros, J., B. Chouet, and P. Dawson (2001a), Spatial extent of a hydrothermal system at Kilauea Volcano, Hawaii, determined from array analyses of shallow long-period seismicity: 2. Results, *J. Geophys. Res.*, *106*, 13,581–13,597.

Almendros, J., B. Chouet, and P. Dawson (2001b), Spatial extent of a hydrothermal system at Kilauea Volcano, Hawaii, determined from array analyses of shallow long-period seismicity: 1. Method, *J. Geophys. Res.*, *106*, 13,565–13,580.

Almendros, J., B. Chouet, and P. Dawson (2002a), Array detection of a moving source, *Seismol. Res. Lett.*, *73*, 153–165.

Almendros, J., B. Chouet, P. Dawson, and C. Huber (2002b), Mapping the sources of the seismic wave field at Kilauea volcano, Hawaii, using data recorded on multiple seismic antennas, *Bull. Seismol. Soc. Am.*, *92*, 2333–2351.

Antolik, M., R. M. Nadeau, R. C. Aster, and T. V. McEvilly (1996), Differential analysis of coda Q using similar microearthquakes in seismic gaps, part 2, Application to seismograms recorded by the Parkfield high resolution seismic network, *Bull. Seismol. Soc. Am.*, *86*, 890–910.

Aster, R. C., and J. Scott (1993), Comprehensive characterization of waveform similarity in microearthquake data sets, *Bull. Seismol. Soc. Am.*, *83*, 1307–1314.

Aster, R. C., G. Slad, J. Henton, and M. Antolik (1996), Differential analysis of coda Q using similar microearthquakes in seismic gaps, part 1, Techniques and application to seismograms recorded in the Anza seismic gap, *Bull. Seismol. Soc. Am.*, *86*, 868–889.

Augliera, P., M. Cattaneo, and C. Eva (1995), Seismic multiplet analysis and its implications in seismotectonics, *Tectonophysics*, *248*, 219–234.

Brancato, A., and S. Gresta (2003), High precision relocation of microearthquakes at Mt. Etna (1991–1993 eruption onset): A tool for better understanding the volcano seismicity, *J. Volcanol. Geotherm. Res.*, *124*, 219–239.

Cattaneo, M., P. Augliera, D. Spallarossa, and C. Eva (1997), Reconstruction of seismogenetic structures by multiplet analysis: An example of Western Liguria, Italy, *Bull. Seismol. Soc. Am.*, *87*, 971–986.

Chouet, B. (1996a), New methods and future trends in seismological volcano monitoring, in *Monitoring and Mitigation of Volcano Hazards*, edited by R. Scarpa and R. Tilling, pp. 23–97, Springer-Verlag, New York.

Chouet, B. (1996b), Long-period volcano seismicity: Its source and use in eruption monitoring, *Nature*, *380*, 309–316.

Chouet, B. (2003), Volcano seismology, *Pure Appl. Geophys.*, *160*, 739–788.

Chouet, B., G. Saccorotti, M. Martini, P. Dawson, G. De Luca, G. Milana, and R. Scarpa (1997), Source and path effects in the wave fields of tremor and explosions at Stromboli Volcano, Italy, *J. Geophys. Res.*, *102*, 15,129–15,150.

Chouet, B., G. De Luca, G. Milana, P. Dawson, M. Martini, and R. Scarpa (1998), Shallow velocity structure of Stromboli Volcano, Italy, derived from small-aperture array measurements of Strombolian tremor, *Bull. Seismol. Soc. Am.*, *88*, 653–666.

Deichmann, N., and M. García-Fernández (1992), Rupture geometry from high-precision relative hypocentre locations of microearthquake clusters, *Geophys. J. Int.*, *110*, 501–517.

Del Pezzo, E., J. M. Ibáñez, and M. La Rocca (1997), Observations of high-frequency scattered waves using dense arrays at Teide volcano, *Bull. Seismol. Soc. Am.*, *87*, 1637–1647.

De Luca, G., R. Scarpa, E. Del Pezzo, and M. Simini (1997), Shallow structure of Mt. Vesuvius Volcano, Italy, from seismic array analysis, *Geophys. Res. Lett.*, *24*, 481–484.

Falsaperla, S., E. Privitera, B. Chouet, and P. Dawson (2002), Analysis of long-period events recorded at Mount Etna (Italy) in 1992, and their relationship to eruptive activity, *J. Volcanol. Geotherm. Res.*, *114*, 419–440.

Ferrazzini, V., K. Aki, and B. Chouet (1991), Characteristics of seismic waves composing Hawaiian volcanic tremor and gas-piston events observed by a near-source array, *J. Geophys. Res.*, *96*, 6199–6209.

Frémont, M. J., and S. Malone (1987), High precision relative locations of earthquakes at Mount St. Helens, Washington, *J. Geophys. Res.*, *92*, 10,223–10,236.

Goldstein, P., and R. Archuleta (1987), Array analysis of seismic signals, *Geophys. Res. Lett.*, *14*, 13–16.

Goldstein, P., and R. Archuleta (1991), Deterministic frequency-wavenumber methods and direct measurements of rupture propagation during earthquakes using a dense array: Theory and methods, *J. Geophys. Res.*, *96*, 6173–6185.

Goldstein, P., and B. Chouet (1994), Array measurements and modeling sources of shallow volcanic tremors at Kilauea Volcano, Hawaii, *J. Geophys. Res.*, *99*, 2637–2652.

Got, J. L., and O. Coutant (1997), Anisotropic scattering and travel time delay analysis in Kilauea volcano, Hawaii, earthquake coda waves, *J. Geophys. Res.*, *102*, 8397–8410.

Got, J. L., J. Frechet, and F. W. Klein (1994), Deep fault plane geometry inferred from multiplet relative relocation beneath the south flank of Kilauea, *J. Geophys. Res.*, *99*, 15,375–15,386.

Haase, J. S., P. M. Shearer, and R. C. Aster (1995), Constraints on temporal variations in velocity near Anza, California, from analysis of similar event pairs, *Bull. Seismol. Soc. Am.*, *85*, 194–206.

Ibáñez, J. M., E. Del Pezzo, J. Almendros, M. La Rocca, G. Alguacil, R. Ortiz, and A. García (2000), Seismovolcanic signals at Deception Island volcano, Antarctica: Wavefield analyses and source modeling, *J. Geophys. Res.*, *105*, 13,905–13,931.

Ibáñez, J. M., J. Almendros, E. Carmona, C. Martínez Arévalo, and M. Abril (2003a), The recent seismo-volcanic activity at Deception Island volcano, *Deep-Sea Res., Part II*, *50*, 1611–1629.

Ibáñez, J. M., E. Carmona, J. Almendros, G. Saccorotti, E. Del Pezzo, M. Abril, and R. Ortiz (2003b), The 1998–1999 seismic series at Deception Island volcano, Antarctica, *J. Volcanol. Geotherm. Res.*, *128*, 65–88.

Ito, A. (1990), Earthquake swarm activity revealed from high-resolution relative hypocenters; clustering of microearthquakes, *Tectonophysics*, *175*, 47–66.

La Rocca, M., S. Petrosino, G. Saccorotti, M. Simini, J. M. Ibáñez, J. Almendros, and E. Del Pezzo (2000), Location of the source and shallow velocity model deduced from the explosion quakes recorded by two seismic antennas at Stromboli Volcano, *Phys. Chem. Earth*, *25*, 731–735.

La Rocca, M., E. Del Pezzo, M. Simini, R. Scarpa, and G. De Luca (2001), Array analysis of seismograms from explosive sources: Evidence for surface waves scattered at the main topographical features, *Bull. Seismol. Soc. Am.*, *91*, 219–231.

Lees, J. (1998), Multiplet analysis at Coso geothermal, *Bull. Seismol. Soc. Am.*, *88*, 1127–1143.

Maurer, H., and N. Deichmann (1995), Microearthquake cluster detection based on waveform similarities with an application to the western Swiss Alps, *Geophys. J. Int.*, *123*, 588–600.

Mezcua, J., and J. Rueda (1994), Earthquake relative location based on waveform similarity, *Tectonophysics*, *233*, 253–263.

Neuberg, J., R. Luckett, M. Ripepe, and T. Braun (1994), Highlights from a seismic broadband array on Stromboli volcano, *Geophys. Res. Lett.*, *21*, 749–752.

Phillips, W. S. (2000), Precise microearthquake locations and fluid flow in the geothermal reservoir at Soultz-sous-Forêts, France, *Bull. Seismol. Soc. Am.*, *90*, 212–228.

Poupinet, G., W. L. Ellsworth, and J. Frechet (1984), Monitoring velocity variations in the crust using earthquake doublets: An application to the Calaveras fault, California, *J. Geophys. Res.*, *89*, 5719–5731.

Poupinet, G., A. Ratdomopurbo, and O. Coutant (1996), On the use of earthquake multiplets to study fractures and the temporal evolution of an active volcano, *Ann. Geofis.*, *39*, 253–264.

Poupinet, G., A. Souriau, and O. Coutant (2000), The existence of an inner core super-rotation questioned by teleseismic doublets, *Phys. Earth Planet. Inter.*, *118*, 77–88.

Press, W., B. Flannery, S. Teukolsky, and W. Vetterling (1992), *Numerical Recipes in Fortran: The Art of Scientific Computing*, 2nd ed., Cambridge Univ. Press, New York.

Ratdomopurbo, A., and G. Poupinet (1995), Monitoring a temporal change of seismic velocity in a volcano: Application to the 1992 eruption of Mt. Merapi (Indonesia), *Geophys. Res. Lett.*, *22*, 775–778.

Saccorotti, G., R. Maresca, and E. Del Pezzo (2001a), Array analyses of seismic noise at Mt. Vesuvius volcano, Italy, *J. Volcan. Geotherm. Res.*, *110*, 79–100.

Saccorotti, G., B. Chouet, and P. Dawson (2001b), Wavefield properties of a shallow long-period event and tremor at Kilauea Volcano, Hawaii, *J. Volcanol. Geotherm. Res.*, *109*, 163–189.

Saccorotti, G., J. Almendros, E. Carmona, J. M. Ibáñez, and E. Del Pezzo (2001c), Slowness anomalies from two dense seismic arrays at Deception Island volcano, Antarctica, *Bull. Seismol. Soc. Am.*, *91*, 561–571.

Saccorotti, G., E. Carmona, and J. M. Ibáñez (2002), Spatial characterization of Agron, southern Spain, 1988–1989 seismic series, *Phys. Earth Planet. Inter.*, *129*, 13–29.

Schmidt, R. (1986), Multiple emitter location and signal parameter estimation, *IEEE Trans. Antennas Propag.*, *34*, 276–280.

Shearer, P. M. (1997), Improving local earthquake locations using the L1 norm and waveform cross-correlation: Application to the Whittier

Narrows, California, aftershock sequence, *J. Geophys. Res.*, *102*, 8269–8284.

Song, X., and P. G. Richards (1996), Seismological evidence for differential rotation of the Earth's inner core, *Nature*, *382*, 221–224.

Stich, D., G. Alguacil, and J. Morales (2001), The relative locations of multiplets in the vicinity of the Western Almería (southern Spain) earthquake series of 1993–1994, *Geophys. J. Int.*, *146*, 801–812.

VanDecar, J. C., and R. S. Crosson (1990), Determination of teleseismic relative phase arrival times using multi-channel cross-correlation and least squares, *Bull. Seismol. Soc. Am.*, *80*, 150–169.

J. Almendros, E. Carmona, and J. Ibáñez, Instituto Andaluz de Geofísica, Universidad de Granada, E-18071-Granada, Spain. (alm@iag.ugr.es)